APSB
Acta Pharmaceutica Sinica B

2021
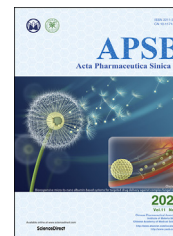
ORIGINAL ARTICLE

TPGS/hyaluronic acid dual-functionalized PLGA nanoparticles delivered through dissolving microneedles for markedly improved chemo-photothermal combined therapy of superficial tumor

Tingting Peng[a], Yao Huang[b], Xiaoqian Feng[b], Chune Zhu[c], Shi Yin[b], Xinyi Wang[d], Xuequn Bai[b], Xin Pan[b,*], Chuanbin Wu[a,b,*]

[a]College of Pharmacy, Jinan University, Guangzhou 510632, China
[b]School of Pharmaceutical Sciences, Sun Yat-sen University, Guangzhou 510006, China
[c]School of Traditional Chinese Medicine, Guangdong Pharmaceutical University, Guangzhou 510006, China
[d]Guanghua School of Stomatology, Hospital of Stomatology, Sun Yat-sen University, Guangzhou 510055, China

Abstract Nanoparticles (NPs) have shown potential in cancer therapy, while a single administration conferring a satisfactory outcome is still unavailable. To address this issue, the dissolving microneedles (DMNs) were developed to locally deliver functionalized NPs with combined chemotherapy and photothermal therapy (PTT). α-Tocopheryl polyethylene glycol succinate (TPGS)/hyaluronic acid (HA) dual-functionalized PLGA NPs (HD10 NPs) were fabricated to co-load paclitaxel and indocyanine green. HD10 NPs significantly enhanced the cytotoxicity of low-dose paclitaxel because of active and mitochondrial targeting by HA and TPGS, respectively. PTT could further sensitize tumor cells toward chemotherapy by promoting apoptosis into the advanced period, highly activating caspase 3 enzyme, and significantly reducing the expression of survivin and MMP-9 proteins. Further, the anti-tumor effects of HD10 NPs delivered through different administration routes were conducted on the 4T1 tumor-bearing mice. After a single administration, HD10 NPs delivered with DMNs showed the best anti-tumor effect when giving chemotherapy alone. As expected, the anti-tumor effect was profoundly enhanced after combined therapy, and complete tumor ablation was achieved in the mice treated with DMNs and intra-tumor injection. Moreover, DMNs showed better safety due to moderate hyperthermia.

*Corresponding authors.
E-mail addresses: panxin2@mail.sysu.edu.cn (Xin Pan), wuchuanb@mail.sysu.edu.cn (Chuanbin Wu).

Therefore, the DMNs along with combined chemo-photothermal therapy provide a viable treatment option for superficial tumors.

1. Introduction

Tumors have become the leading cause of the threat to health and death in humans. Chemotherapy is the most widely used and classical clinical regimen for cancer therapy. However, some malignant tumors, such as triple-negative breast cancer (TNBC) and melanoma, are insensitive to conventional chemotherapy, and thus, some combination therapies are urgently needed to improve the efficacy of chemotherapy. Recently, the combination of chemotherapy and photothermal therapy (PTT) mediated by nanoparticles (NPs) has emerged as a new modality for tumor treatment, since NPs are uniquely advantageous in controlling drug release, improving drug efficacy, and enhancing photothermal effect.

Among diverse nanocarriers, poly (lactic-*co*-glycolic acid) (PLGA) NPs have gained great attention due to their desirable properties of good biocompatibility, versatile modification, and simple production[1,2]. However, bare PLGA NPs with strong hydrophobicity usually involves several drawbacks, including (1) easy recognition and uptake by the reticuloendothelial system, leading to a short circulation time *in vivo*[3], (2) poor adhesion to cells and low permeability to the cell membrane[4], and (3) low encapsulation efficiency of hydrophilic drugs[5].

To address the intrinsic dilemma, surface modification of PLGA NPs with poly (ethylene glycol) (PEG)[6,7], lipids (lecithin, DSPE-PEG)[8], or surfactants α-tocopheryl polyethylene glycol succinate (TPGS)[9,10], poloxamer[11] and enclosure of PLGA NPs with cell membranes (erythrocyte[12], platelet[13], and cancer-derived cells[14]) are commonly used strategies. Obviously, it was more feasible to modify PLGA NPs using the commercially available materials, rather than the naturally derived lipids. Until now, there has been no report on the use of TPGS-functionalized PLGA NPs to co-deliver chemotherapeutic drug and photosensitizer for combined chemo-photothermal therapy. TPGS also offers unique advantages over other PEGylated material or lipids by targeting mitochondria to trigger cell apoptosis and amplifying the apoptosis-inducing effect of PTT[15,16]. Therefore, we conjecture that the TPGS-modified PLGA NPs with combined chemo-photothermal therapy can maximize the anti-tumor efficacy to the fullest.

Herein, indocyanine green (ICG) and paclitaxel (PTX) were used as the photosensitizer and chemotherapeutic drug, respectively. Unfortunately, the conventional PLGA NPs showed a relatively low encapsulation efficiency of ICG at about 20%−40%[5,8]. Therefore, a cationic lipid 1,2-dioleoyl-3-trimethylammonium-propane (DOTAP) was introduced to provide a positively charged surface to the hybrid NPs and further increase the encapsulation efficiency (EE%) of negatively charged ICG. Hyaluronic acid (HA) with the negative charge was further used to coat the hybrid NPs, and hence neutralize the positive charge of NPs to avoid plasma adsorption and rapid clearance from blood circulation[17,18]. Meanwhile, the HA-coated hybrid NPs are expected to achieve active tumor targeting by specifically interacting with CD 44 receptors, which are overexpressed on many types of tumor cells[18−20]. However, multiple and frequent injections of these NPs at high dosage are commonly required to achieve a satisfying anti-tumor outcome, which may cause severe adverse effects and patient discomfort.

The recent development of dissolving microneedles (DMNs) has revolutionized the treatment modality of superficial tumors because it provides a platform for local treatment with reduced dosing, enhanced safety, and promising anti-tumor outcome[21−24]. Compared to intravenous and intratumor injections, DMNs, which contain multiple needles as drug depots, are more susceptible to releasing cargoes and realizing uniform heat distribution from PTT over tumors, thus diminishing tumor recurrence and inferior outcome.

Based on this, our study aimed to develop composite DMNs loading NPs, with the advantages of both polymeric NPs and DMNs, for treating superficial tumors with a combination of chemotherapy and PTT. We firstly constructed the TPGS/HA dual-functionalized PLGA NPs and evaluated the underlying cell apoptotic mechanism. Next, mixtures of polyvinylpyrrolidone (PVP) and polyvinyl alcohol (PVA) were used as needle material to prepare NPs-loaded DMNs because of their hydrophilic nature and appropriate mechanical strength[25,26]. Finally, we established the animal model of 4T1 tumor-bearing mice to compare the anti-tumor efficacy of NPs delivered through tail vein injection, intratumor injection, and DMNs.

2. Materials and methods

PTX (purity>99%, MW = 853.91), coumarin-6, TPGS and PVA-103 were purchased from Sigma−Aldrich (St. Louis, MO, USA). Free-acid terminated PLGA (MW = 5000−15,000 Da) with a 50:50 monomer ratio was gained from Daigang Biological engineering Co., Ltd. (Jinan, China). ICG (laser grade) was procured from Acros Organics (Belgium, USA). 1,2-Dioleoyl-3-trimethylammonium-propane (DOTAP) was obtained from Avanti Polar Lipid, Inc. (Alabaster, AL, USA). Small molecular HA (purity>99%, MW = 10,000) was obtained from Ronlabs Co., Ltd. (Shanghai, China). PVP K30 and K90 was kindly donated by BASF AG (Shanghai, China). Dulbecco's modified Eagle's medium (DMEM, Gibco™) and fetal bovine serum (FBS, Gibco™) were obtained from Thermo Fisher Scientific (MA, USA). Cell Counting Kit-8 (CCK-8) was gained from Dojindo Molecular Technologies, Inc. (Kyushu, Japan). Caspase 9 and 3 activity assay kits were obtained from Biyotime Biotechnology Co., Ltd. (Shanghai, China). Annexin V-FITC/propidium iodide (PI) apoptosis detection kit was purchased from Lianke
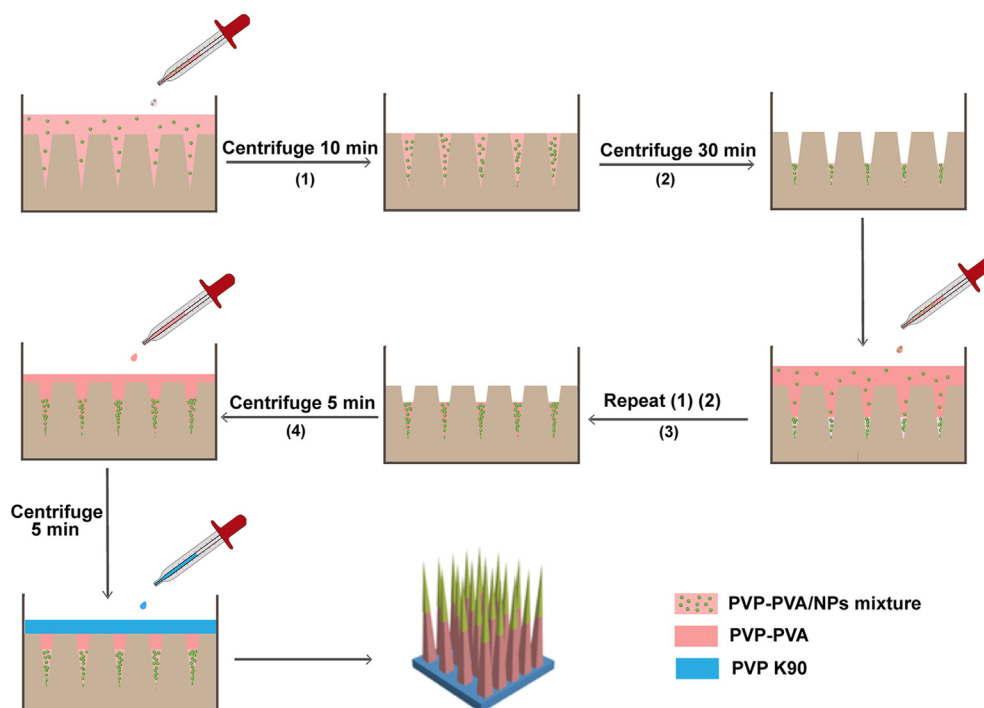
Figure 1   Schematic illustration of preparing HD10 NP-loaded DMNs.

Biotechnology Corp. Ltd. (Hangzhou, China). All other reagents were used as received.

2.1.   Preparation and characterization of TPGS and TPGS/HA functionalized PLGA NPs

TPGS-modified PLGA NPs [termed as D10 NPs, with 10% (w/w) DOTAP of polymer weight] were prepared by the nanoprecipitation method. Briefly, PLGA (3.6 mg/mL), DOTAP (0.4 mg/mL), and PTX (0.2 mg/mL) dissolved in acetone were used as the organic phase. The mixtures of TPGS (2.0 mg/mL, 2.5 mL) in 4% (w/w) ethanol aqueous solution, and ICG (1.0 mg/mL, 100 μL) in 20% (v/v) methanol aqueous solution were used as the aqueous phase and heated to 65 °C. D10 NPs were generated by dripping 0.5 mL of acetone solution dropwise into the aqueous solution under magnetic stirring (Magnetic Stirrer, WH-610D) for 20 min at 35 °C. Then, HD10 NPs were prepared by slowly adding HA solution (1 mg/mL) into the fresh D10 NPs at a 2:3 volume ratio, depending on the electrostatic force between HA and D10 NPs. Finally, the residual organic solvent and free PTX or ICG were removed by washing the D10 NPs or HD10 NPs thrice using an Amicon Ultra-4 centrifugal filter (MWCO 10 kDa, Millipore, Billerica, MA, USA). The resultant NPs were stored in the dark at 4 °C until further use.

Characterization of NPs in terms of particle size, zeta potential, EE%, morphology, spectroscopic properties, fluorescent intensity, photothermal effect, and in vitro drug release study, is provided in the Supporting Information.

2.2.   Cellular study

The cytotoxicity evaluation of different formulations with or without laser irradiation (LS) was carried out on the MDA-MB-231 cells. The mechanism of cell death induced by chemotherapy or chemo-photothermal combined therapy was investigated by determining apoptosis, intracellular localization, caspase 3 and 9 activity, and the expression of proteins related to tumor metastasis or recurrence. Detailed evaluations are provided in the Supporting Information.

2.3.   Preparation and characterization of DMNs

DMNs were prepared by a stepwise centrifugation method to concentrate the NPs in the tip of needles and increase the dug loading of DMNs (Fig. 1)[27]. The detailed procedure and characterization of DMNs in terms of morphology, skin insertion ability, and photothermal conversion efficiency are provided in the Supporting Information.

2.4.   In vivo studies

The 4T1 tumor-bearing mice with tumors of 100−150 mm³ volume were used to evaluate and compare the in vivo photothermal effect and anti-tumor efficacy of different administration routes (intravenous injection, intra-tumor injection, and DMNs) of HD10 NPs. Major organs were histologically evaluated to determine the safety of various treatments. All animal experiments were conducted under the protocols approved by the Institution Animal Care and Use Committee of Sun Yat-sen University, Guangzhou, China (Approval No. SYSU-IACUC-2019-000114). Detailed information is summarized in the Supporting Information.

2.5.   Statistical analysis

Data are reported as mean±standard deviations (SD). For multiple comparisons, data were analyzed by one-way analysis of variance (ANOVA) with Turkey's test (for pairwise comparison with each other) or Dunnett's test (with the untreated or defined group as a control) using GraphPad Prism 7.0 software (GraphPad Software
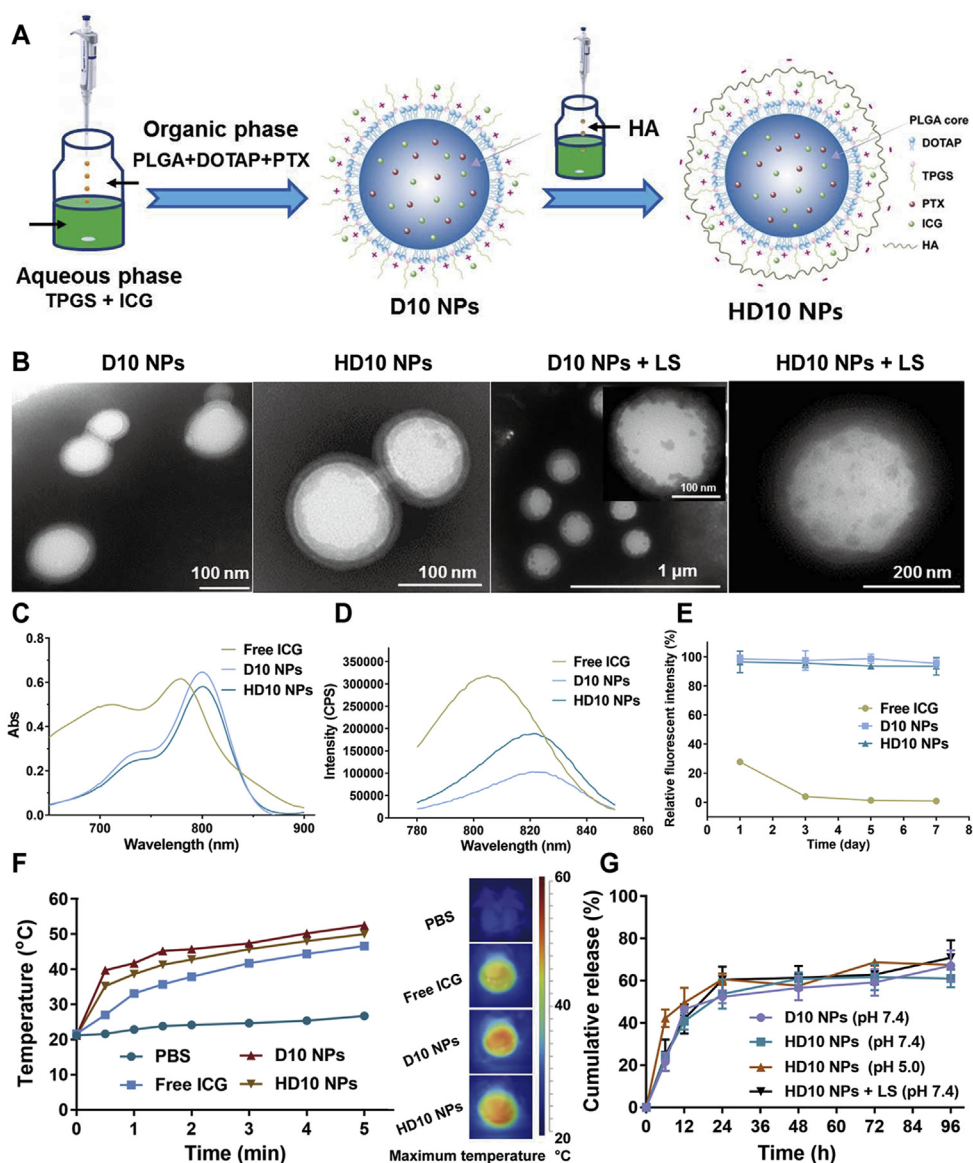
Figure 2 Preparation and characterization of D10 NPs and HD 10 NPs: (A) the schematic illustration of preparing D10 NPs by nano-precipitation and HD 10 NPs by titration, (B) TEM morphology of NPs before and after LS, (C) UV−Vis absorbance spectra, (D) the fluorescence emission spectra, (E) the fluorescent stability of free ICG, D10 NPs and HD10 NPs aqueous solution incubated at 37 °C over 7 days (Data are presented as mean ± SD, $n = 3$), (F) *in vitro* photothermal effect, and (G) *in vitro* drug release profiles (Data are presented as mean ± SD, $n = 3$).

Inc., San Diego, CA, USA). Differences with $P < 0.05$ were considered statistically significant.

3. Results and discussion

3.1. Preparation and characterization of NPs

The schematic illustration of D10 and HD10 NPs preparation is displayed in Fig. 2A. D10 NPs were prepared by nano-precipitation, where the organic phase loading PLGA/DOTAP/PTX was slowly added to the aqueous solution containing TPGS/ICG. PLGA was precipitated with the diffusion of the organic solvent into the aqueous solution, to form the polymer matrix, while DOTAP and TPGS were simultaneously aligned and deposited around the PLGA core due to their amphiphilic nature. As a consequence, D10 NPs with a core−shell structure was

formed. Then, HD10 NPs with a core−shell−shell structure were prepared by HA coating of D10 NPs by electrostatic crosslinking.

3.1.1. Particle size, zeta potential, and encapsulation efficiency of NPs

The particle size, zeta potential, and encapsulation efficiency (EE, %) of NPs are presented in Table 1. D10 NPs and H10 NPs had a particle size of about 140 and 160 nm, respectively. The zeta potential of D10 NPs was 9.20 mV, while that of HD10 NPs shifted to −19.40 mV. The increased particle size and negative charge of HD10 NPs confirmed the adsorption of HA onto the D10 NPs. Both D10 and H10 NPs showed an EE% of PTX (>85%) and ICG (>47%). PTX could be effectively encapsulated into the PLGA core, since TPGS has a good solubilizing ability to PTX, and PLGA interacted with PTX through a hydrophobic force. When the mass ratio of TPGS/PLGA was ≥3, the EE% of

Table 1 The physical characteristics of D10 NPs and HD 10 NPs.

NP	Z-average (nm)	PDI	Zeta potential	EE (%)	
			(mV)	PTX	ICG
D10 NPs	142.40 ± 4.30	0.14 ± 0.01	9.20 ± 0.17	87.01 ± 1.11	50.23 ± 4.14
HD10 NPs	162.30 ± 1.80	0.15 ± 0.01	-19.40 ± 0.79	85.93 ± 4.29	47.43 ± 1.89

Data are presented as mean $\pm$ SD ($n = 3$).

PTX was up to 85%[10]. The potential causes for high EE% of ICG were (1) ICG being an amphiphilic compound, can not only be encapsulated into PLGA core through hydrophobic interaction with PLGA but also form a self-assembled complex with TPGS to deposit as the outer shell[28]; (2) the positively charged DOTAP in the shell can adsorb ICG *via* electrostatic force (the amount of DOTAP in the physicochemical properties of NPs is described in Supporting Information Fig. S2); (3) ICG and PTX can interact with each other through the electrostatic force and $\pi-\pi$ stacking, which further improved the EE% of ICG[29].

3.1.2. Morphologies of NPs before and after LS

The morphologies of NPs before and after LS are shown in Fig. 2B. D10 NPs show a well-defined spherical shape with a core–shell structure, indicating the successful coating of PLGA core by TPGS shell and a good agreement with the outcomes of a previous report[10]. The core–shell–shell structure of HD10 NPs further confirmed the successful coating of D10 NPs with HA by electrostatic interaction. However, after LS, the outer TPGS shell showed noticeable ablation, while the PLGA core remained intact or showed slight ablation. This was mainly because the melting point of TPGS (41.6 °C) is relatively low; however, the increased temperature during LS was insufficient to corrode the PLGA core to split it into smaller pieces.

3.1.3. Spectroscopic properties

Compared to the free ICG solution, the absorption spectra of ICG-loaded NPs exhibited a red-shift from 778 to 800 nm (Fig. 2C), which agreed well with previous studies[30,31]. Likewise, the fluorescence emission spectrum of ICG-loaded NPs (Fig. 2D) red-shifted from 805 to 822 nm at the excitation wavelength of 763 nm.

3.1.4. Fluorescent intensity

The fluorescence intensity decreased to 27.8% and 4.0% of its initial value on the 1st and 3rd day, respectively (Fig. 2E). It was reported that ICG had poor stability and could degrade to its free form because ICG concentration exceeding 2 μg/mL could cause its self-quenching by forming aggregated particles through the van der Waals force and hydrophobic interaction force between the ICG molecules[32]. The relative fluorescence intensity of ICG loaded NPs was more than 94% during storage, indicating that encapsulation of ICG into the NPs successfully avoided rapid aggregation, degradation, and self-quenching in aqueous solution, thereby remarkably improving the fluorescence stability of the ICG aqueous solution[33,34].

3.1.5. In vitro photothermal effect

The temperature changes and typical thermal images of different solutions during LS are presented in Fig. 2F. The temperature of all solutions except PBS increased with an increase in irradiation time. The highest temperature of PBS, free ICG, D10 NPs, and HD10 NPs was 26.7, 46.6, 52.5 and 50 °C, respectively, showing

that the encapsulation of ICG in NPs increased the photothermal conversion efficiency of ICG. The major reasons for enhanced heating efficacy of NPs were: (1) increased photothermal stability of ICG[35], (2) higher local ICG concentration from NPs[31], (3) closer absorption peak of ICG-loaded NPs to 808 nm resulting in more efficient heat production[36].

3.1.6. In vitro drug release profiles

The *in vitro* release profiles of various NPs are shown in Fig. 2G. The release rates of D10 and HD10 NPs were comparable, indicating that HA coating of D10 NPs did not affect the diffusion of PTX from the NPs into the dissolution buffer because HA could dissolve rapidly upon contact with dissolution buffer. However, the release rate of HD10 NPs after LS increased slightly, possibly due to the minor ablation in the PLGA core. While on the one hand, HD10 NPs did not show sensitive light-triggered release behavior, on the other hand, PEGylation of PLGA NPs with TPGS did not hinder the contact of PLGA with the release medium and delayed drug release, while drug release retardation with PEGylated PLGA NPs has been reported in previous studies[37,38]. Additionally, at pH 5.0, HD10 NPs exhibited remarkably faster drug release within 12 h than that at pH 7.4, probably due to increased PLGA degradation in acidic medium[39].

3.2. Cellular study of NPs

3.2.1. Cell viability

The cell viability of MDA-MB-231 cells with different treatments is shown in Fig. 3A–C, and the determination of half-maximal inhibitory concentration (IC_{50}) of PTX is displayed in Table 2. The cytotoxicity of PTX was significantly enhanced after D10/HD10 NP encapsulation. This was attributed to the increase in the cellular uptake of PTX, and TPGS-mediated synergistic inhibition of cell proliferation with PTX by reducing drug efflux as an inhibitor of P-gp[40,41], and activation of mitochondrial apoptotic pathways in cells with enhanced intracellular ROS generation, mitochondrial depolarization, and functional degradation[42,43]. There was no significant difference in the 24 h cytotoxicity of D10 and HD10 NPs, while the 48 h cytotoxicity was greater in HD10 NPs than in D10 NPs at low-dose PTX (0.001–0.1 μg/mL). This may be because HA recognized the highly expressed CD44 receptor on MDA-MB-231 cells, and increased the uptake of NPs by receptor-mediated endocytosis[44].

Irrespective of formulation and dosage, the chemo-photothermal combined therapy displayed higher cytotoxicity than the chemo-monotherapy (Fig. 3C). The mechanism of PTT enhancing the cytotoxicity of PTX occurred primarily in two ways: (1) the generated heat could rupture lysosomes and further induce programmed cell apoptosis[45], and (2) the produced ROS, such as hydroxyl and singlet oxygen, damaged the cells by inducing necrosis[46,47]. This enhancing effect was more noticeable in the D10/HD10 NPs than in free PTX/ICG, implying that incorporation of ICG in NPs could augment the anti-tumor

efficacy of PTT due to increased photothermal conversion efficiency and cellular uptake.

3.2.2. Cell apoptosis

Cell apoptosis was quantified by flow cytometry. As shown in Fig. 3D, the ability of different treatments to induce apoptosis followed the order of HD10 NPs + LS > HD10 NPs > D10 NPs + LS > D10 NPs > Free PTX + ICG + LS > Free PTX + ICG. The result indicates that the encapsulation of PTX in NPs, especially in HD10 NPs, profoundly enhanced the apoptotic effect. Also, the combination of chemotherapy and PTT showed remarkably enhanced apoptosis-inducing capacity in comparison to chemotherapy alone, which is consistent with the result of cytotoxicity evaluation. Interestingly, PTT induced more cells to enter the late apoptosis for the D10 and HD10 NPs, but more cells to the early apoptosis for the free PTX/ICG.

3.2.3. Subcellular localization of the NPs

The mitochondrial specificity of D10/HD10 NPs was monitored using confocal laser scanning microscopy (CLSM). Free coumarin-6 and coumarin-6 loaded D10/HD10 NPs displayed an intrinsic green fluorescence, and Mitotracker Deep Red was used to label mitochondria with red fluorescence. According to Fig. 4A−C, free coumarin-6 displayed a distinguished separation from the mitochondria but presented a high co-localization with

Table 2 Inhibitory concentration (IC_{50}) of PTX in MDA-MB-231 cells.

Formulation	IC_{50} (µg/mL)	
	24 h	48 h
Free PTX	>10	0.02211
D10 NPs	0.1008	0.01221
HD10 NPs	0.1248	0.00312

lysosomes (Supporting information Fig. S5), indicating that free coumarin-6 could internalize into the cells and get entrapped by the lysosome. An opposite phenomenon was observed in the D10/HD10 NPs, where the green fluorescence signal overlapped well with the red fluorescence signal, resulting in a strong yellow fluorescence signal. This result demonstrates the primary accumulation of NPs in the mitochondria after cellular uptake. The mitochondrial targeting capacity of the NPs could be benefited from the TPGS coating, as an outer shell of NPs[42], and the positively charged DOTAP, recruiting the NPs to the negatively charged mitochondrial site by electrostatic interaction[48].

3.2.4. Caspase activation

Caspase activation is closely linked to the apoptosis in mitochondria[49]. The activation of caspases 9 and 3 act as the initiator
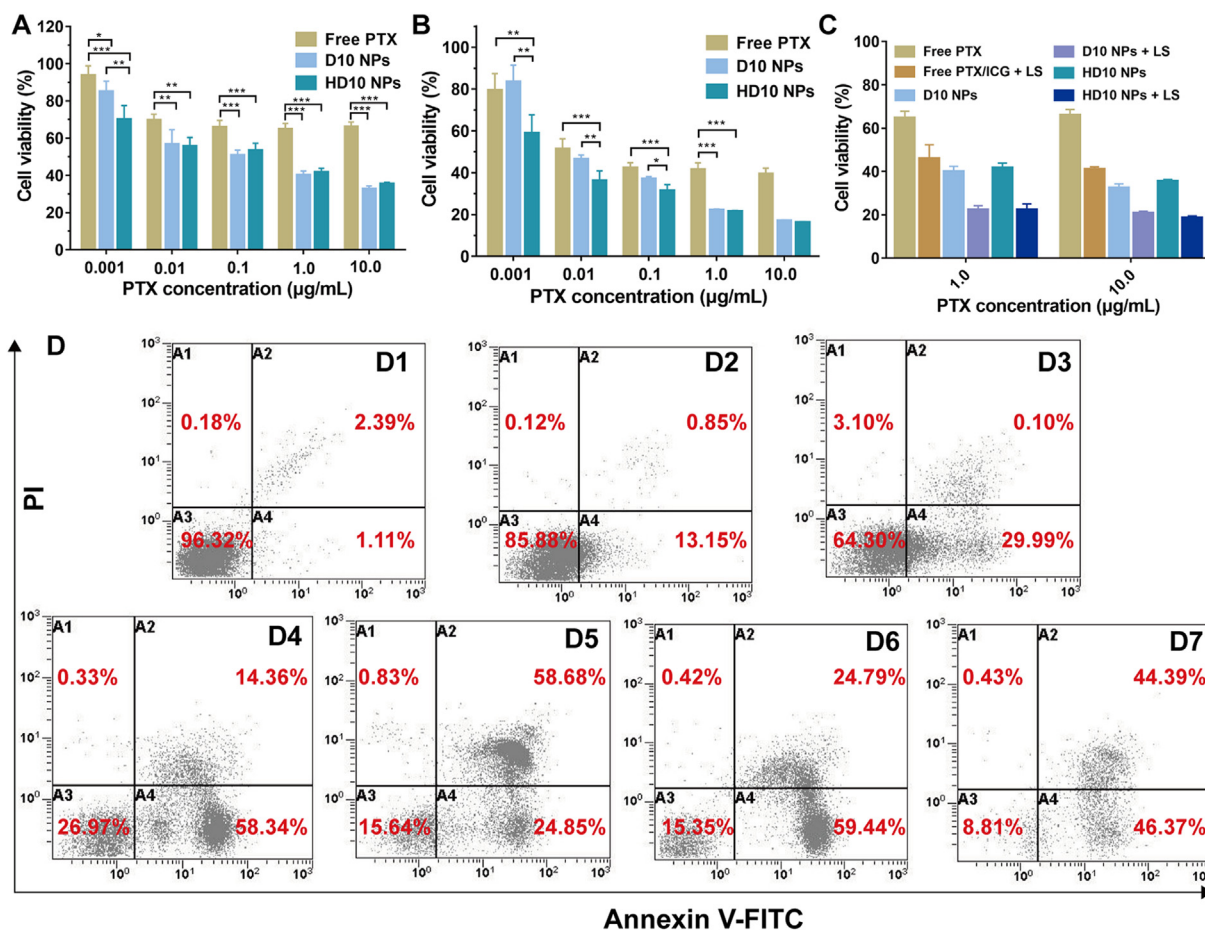

Figure 3 Cytotoxicity evaluation of MDA-MB-231 cells incubated with different formulations. Cell viability at 24 h (A) and 48 h (B) without LS, and 24 h with LS (C). Data are presented as mean ± SD ($n = 5$), *$P < 0.05$, **$P < 0.05$ and ***$P < 0.001$. (D) Cell apoptosis detected by the flow cytometry: (D1) untreated group, (D2) free PTX + ICG, (D3) free PTX + ICG + LS, (D4) D10 NPs, (D5) D10 NPs + LS, (D6) HD10 NPs, and (D7) HD10 NPs + LS.
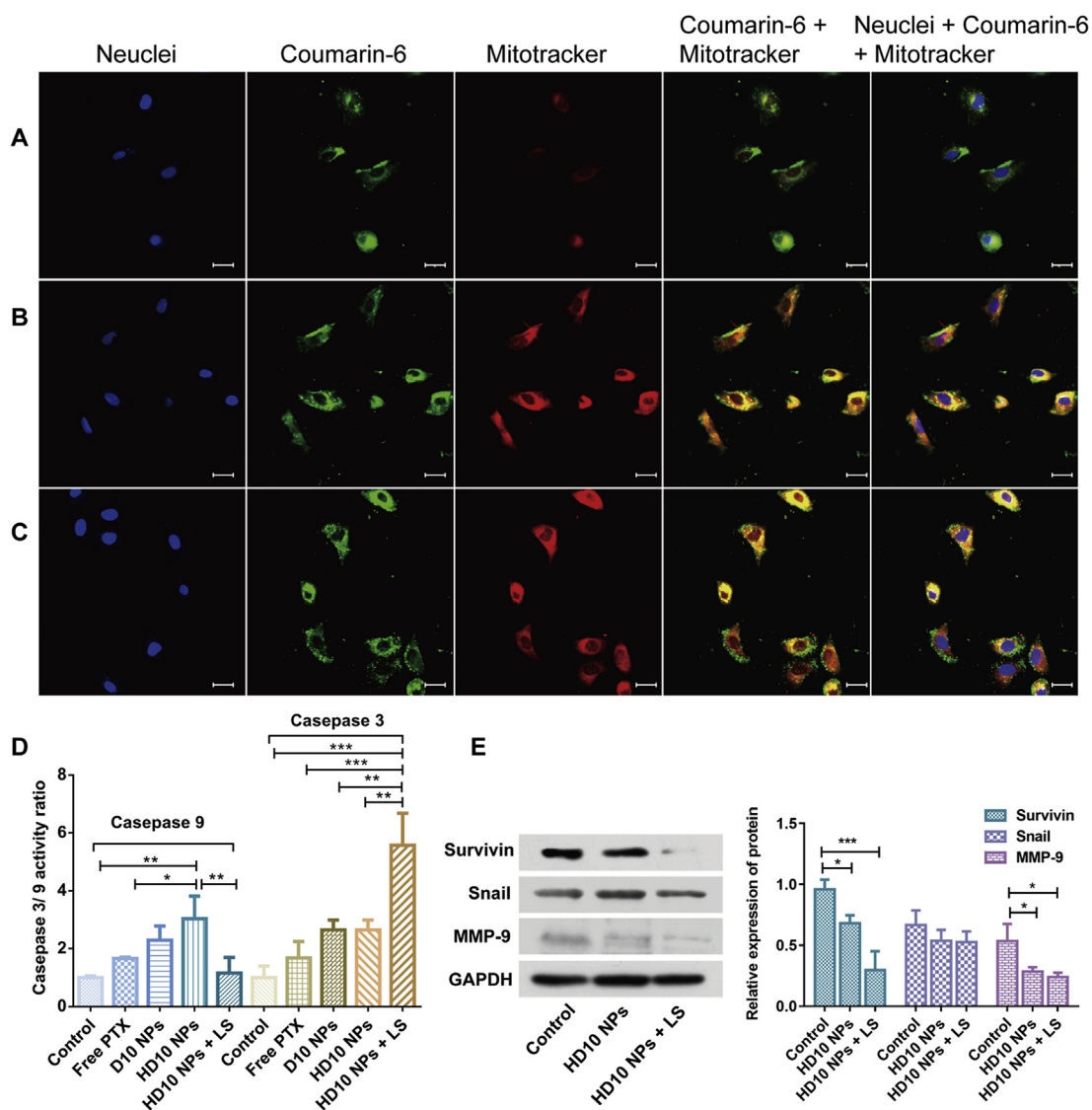
Figure 4 The distribution of coumarin-6 in the nucleus and mitochondria of MDA-MB-231 cells after treatment with free coumarin-6 (A), D10 NPs (B), and HD10 NPs (C). Scale bar = 30 μm. (D) and (E) Mechanistic investigation of apoptosis in the MDA-MB-231 cells after receiving different treatments. (D) Caspases 9 and 3 activations and (E) the relative protein expression of surviving, snail and MMP-9 protein. Data are presented as mean ± SD (n = 3), *$P < 0.05$, **$P < 0.05$ and ***$P < 0.001$.

and ultimate effector in the cascade reaction, respectively[50]. In general, D10 and HD10 NPs enhanced the activity of caspases 9 and 3 much better than free PTX (Fig. 4D). The activity ratio of caspase 9 in the cells treated with HD10 NPs showed a 1.82-fold and 1.33-fold of free PTX and D10 NPs, respectively. A similar trend was also found in the activity of caspase 3, and HD10 NPs showed the highest activity ratio when the cells were subject to chemotherapy alone. It was demonstrated that TPGS/HA dual-functionalized NPs were more capable in inducing apoptosis than TPGS single functionalized NPs. Although the activity ratio of caspase 9 in the cells treated with HD10 NPs and LS was significantly lower than that of HD10 NPs, the caspase 3 activity ratio of the HD10 NPs with LS group was 2.1-fold of HD10 NPs. This result further confirms that the combination of chemotherapy and PTT greatly elevated the cellular caspase 3 activity, and promoted the cells to advance into the late apoptosis.

3.2.5. Western blotting

The expression of proteins related to the invasion, metastasis, and prognosis of TNBC was evaluated by Western blotting (Fig. 4E). Compared with normal cells, the expression of MMP-9 was significantly reduced in cells treated with HD10 NPs or HD10 NPs plus LS. MMP-9 is one of the extremely crucial proteolytic enzymes involved in cell invasion and migration for the degradation of the extracellular matrix and basement membrane[51]. Besides, snail overexpresses in the MDA-MB-231 cells[52], as a member of the upstream transcription factors during epithelial−mesenchymal transition (EMT), and participates in the invasion and migration of tumor[53]. However, the expression of snail did not show a noticeable reduction after treatment with either chemotherapy or chemo-photothermal combined therapy. However, the expression of survivin was significantly reduced after giving LS, consistent with the outcomes of the previous report[54]. Survivin is known to
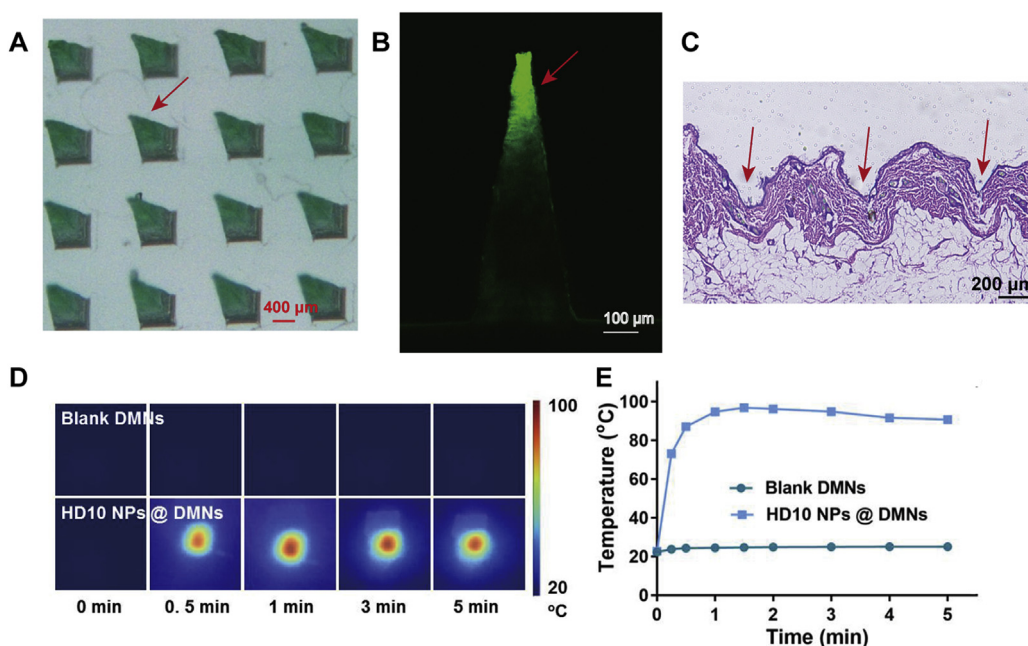
Figure 5 Characterization of HD10 NPs loaded DMNs: (A) bright-field photograph under a stereo fluorescence microscope, (B) CLSM image, (C) H&E-stained skin histologic section to evaluate skin insertion ability, (D) near-infrared thermal imaging and (E) the maximum temperature change curves of blank DMNs and HD10 NPs loaded DMNs under LS to assess the *in vitro* photothermal conversion efficiency.

mediate the metastasis and prognosis of TNBC, and the decrease in its expression was advantageous in terms of suppressed tumor metastasis[55] and sensitized cancer cells toward chemotherapeutic drugs[56]. These results, therefore, suggest that the combination of chemotherapy and PTT could not only lower tumor invasion and metastasis but also potentially improve TNBC prognosis.

3.3. Characterization of DMNs loading NPs

The fabricated array of DMNs had a regular pyramid shape with a needle height approaching 800 μm (Fig. 5A). Besides, only the needle tip was in green color and showed green fluorescence (Fig. 5B). Since the ICG-loaded NPs are green and emit green fluorescence at the excitation wavelength of 675 nm, it was deduced that NPs were successfully enriched in the needle tip. Such DMNs are conducive to delivering drugs to the dermis and avoiding waste of drug residues on the skin surface.

The Hematoxylin & Eosin (H&E) staining of the punctured skin (Fig. 5C), revealed that obvious microchannels were created in the skin with DMNs application, and the insertion depth was 250−350 μm, available to reach the dermis for efficient drug delivery. Therefore, the produced DMNs exhibited good skin penetration ability. Besides, the far shorter insertion depth than the height of DMNs could be ascribed to two aspects[57]: (1) the inserted skin could shrink due to its elasticity, and (2) the needle tips adsorbed physiological fluid and dissolved quickly (Supporting Information Fig. S6).

The temperature increase of DMNs during LS (Fig. 5D and E) was used to evaluate their photothermal conversion capacity. The blank DMNs showed a slightly increased temperature during LS, with a maximum temperature increase of 2.8 °C, indicating that the preparation material of DMNs basically did not exert heating

capacity. However, the temperature of HD10 NPs containing DMNs increased rapidly to 94.7 °C within 1 min after LS, and the temperature could be maintained above 90 °C for 4 min. These results indicate that DMNs loaded with NPs have excellent photothermal conversion efficiency, which further benefits to ensure the heating efficiency *in vivo*. Furthermore, the superiority of DMNs to HD10 NPs solution in heating efficacy implies that the enrichment of in the needle offered a feasible way to improve the photothermal conversion efficiency of ICG. The reason for this could be the soild-state of the NPs loaded in the DMNs, which benefits by increasing the photostability and local concentration of ICG than that in the solution state.

3.4. In vivo study of NPs and DMNs

3.4.1. In vivo photothermal effect

For a guarantee *in vivo* anti-tumor effect, an effective increase in temperature is essential. As shown in Fig. 6A and B, all groups showed the increased temperature in the local tumor, with the order of maximum temperature as intratumoral injection group > DMNs group (two patches) > DMNs (one patch) > caudal vein injection > untreated group, corresponding to an average temperature of 60.6, 53.7, 50.5, 48.9, and 40.4 °C. Concurrently, the temperature of untreated mice during LS did not exceed 41 °C, which was insufficient to promote tumor cell apoptosis for effective PTT. The temperature of both intratumoral injection and DMNs group exceeded the threshold (above 50 °C) required to cause irreversible damage to the tumor[58], while the higher temperature achieved in the intratumoral injection group could result from a higher dose of ICG (5.4-fold to the single DMNS patch). Nevertheless, DMNs exhibited an excellent heating efficiency, as one DMN patch contained only 4.1 μg of ICG. In the
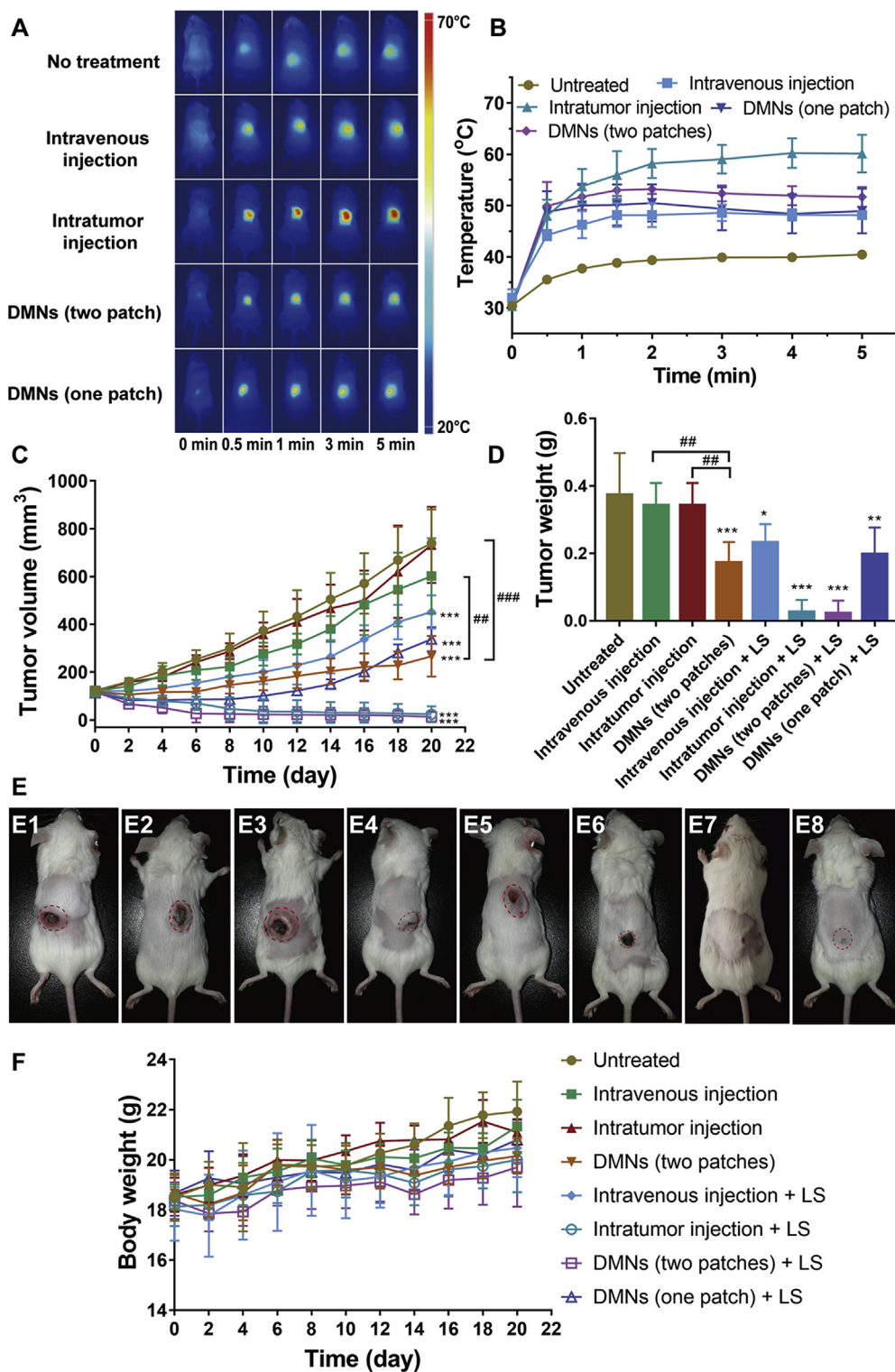
Figure 6 Anti-tumor effect of HD10 NPs delivered with different administration routes. (A) *In vivo* near-infrared thermal imaging of mice receiving LS, (B) the temperature change curves of local tumors, (C) the tumor volume growth curve of 4T1 tumor-bearing mice within 20 days, (D) the tumor weight of mice on Day 20 post-administration, (E) the photographic images of the mice on Day 20 post-administration, which were successively designated as untreated group (E1), intravenous injection (E2), intratumor injection (E3), DMNs (two patches) (E4), intravenous injection + LS (E5), intratumor injection + LS (E6), DMNs (two patches)+LS (E7), and DMNs (one patch)+LS (E8), and (F) the change in body weight of 4T1 tumor-bearing mice within 20 days. Data are presented as mean $\pm$ SD for A ($n = 3$), B, C and E ($n = 5$). $*P < 0.05$, $**P < 0.01$ and $***P < 0.001$ *vs.* the untreated group. $^{\#\#}P < 0.001$ and $^{\#\#\#}P < 0.001$ indicates the pairwise comparision of the intravenous injection, the intratumor injection and the DMNs, when chemotherapy alone was conducted.
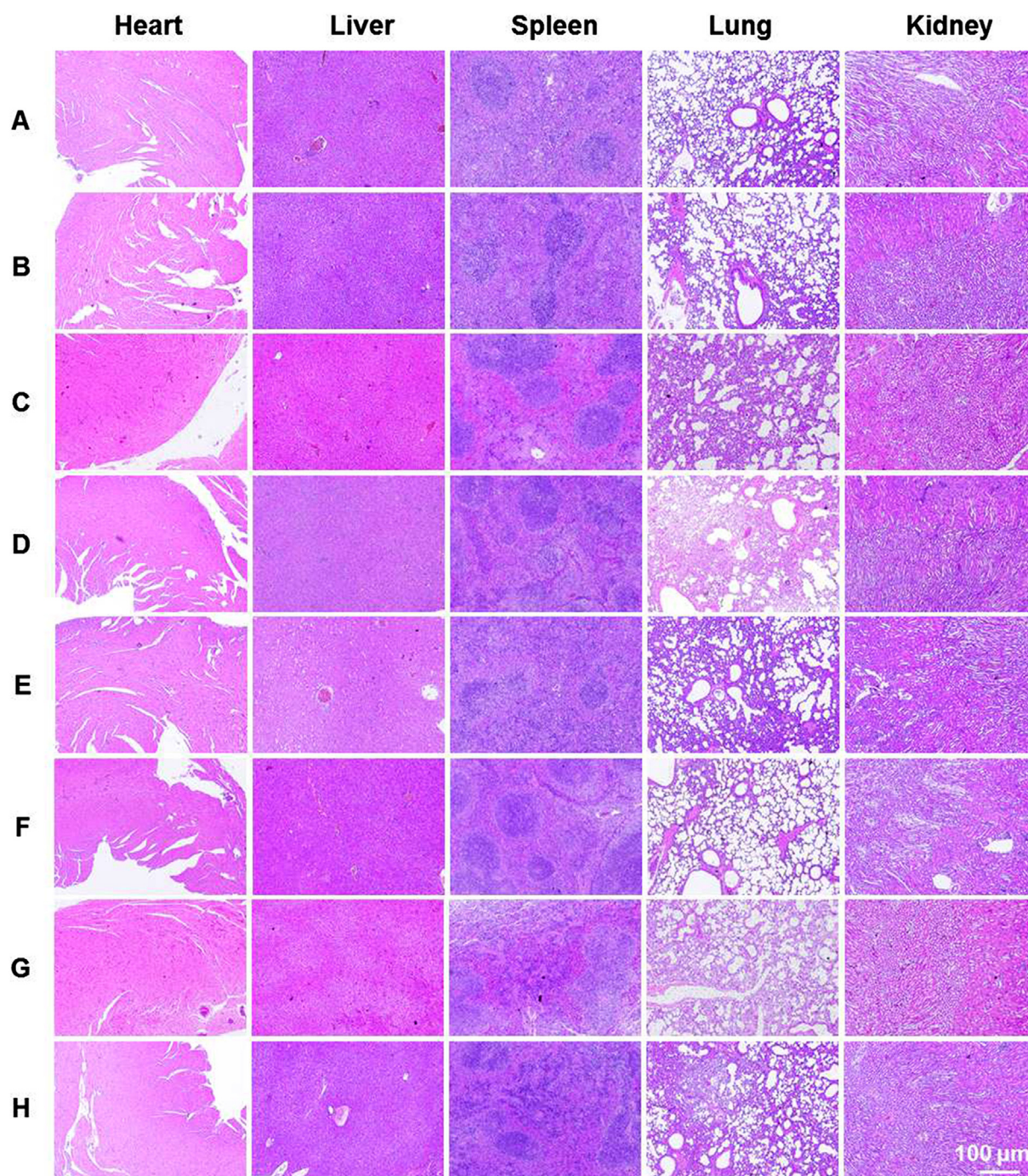
Figure 7 The H&E staining images of major organs extracted from the mice receiving different treatments: (A) untreated, (B) intravenous injection, (C) intratumor injection, (D) DMNs (two patches), (E) intravenous injection + LS, (F) intratumor injection + LS, (G) DMNs (two patches)+LS, and (H) DMNs (one patch)+LS.

caudal vein injection group, the temperature was elevated up to 45−50 °C, which could produce certain damage to tumor cells and risk of tumor recurrence[35], as well as a successful accumulation of ICG in the tumor (Supporting Information Fig. S7). The inferior heating efficiency of caudal vein injection to DMNs maybe because the NPs through caudal vein injection could distribute throughout the whole body and dramatically diminish the ICG concentration before reaching the tumor tissue, while DMN is an *in situ* administration route that allows the NPs with condensed ICG to be released locally for highly efficient heat generation.

3.4.2.   *In vivo anti-tumor effect*

The therapeutic efficacy of HD10 NPs *via* different administration routes was compared and assessed on the 4T1-tumor-bearing mice. The tumor volume growth profile and tumor weight at the endpoint of the experiment are displayed in Fig. 6C and D, respectively. Compared with the untreated group, intratumorally injected HD10 NPs showed no anti-cancer effect because only one dosing was given, and most of the drug could leak into the surrounding subcutaneous tissue. Injection of HD10 NPs *via* caudal vein had a minimal inhibitory effect on tumor growth, which may

be because the NPs enriched in the tumor tissue exerted certain tumor-suppressing effects in the early stage. This was consistent with earlier reports that the chemo-monotherapy by PTX is insensitive toward TNBC, and frequent injections are required to achieve a considerable anti-tumor effect[59,60]. Additionally, HD10 NPs delivered through DMNs significantly lowered the tumor growth rate, resulting in tumors of the average volume of 266 mm^3 on Day 20. Overall, the capacity of different administration routes to suppress tumor growth followed the order of DMNs > tail vein injection > intratumoral injection. The greatest anti-cancer efficacy of DMNs could be the uniform and broad dispersion of PTX in the tumor tissue to maximize its anti-tumor effect without wastage due to drug leakage.

When chemotherapy and PTT were simultaneously administered, the tumor growth inhibition rate was further strengthened irrespective of the administration route. PTT enhanced the effect of chemotherapy by producing hyperthermia and destroying cancer cells. More importantly, most of the mice in the DMNs (two patches) group and the intratumoral injection group were completely ablated, mainly due to effectively localized PTT. However, we should bear in mind that the efficacy of PTT was also affected by dosage, as the single DMN patch group could effectively prohibit tumor growth in the early stage, but tumor regrew continuously after the 10th day, probably due to insufficient damage to cancer cells. Furthermore, in the mice receiving an intratumoral injection, skin tissue around tumor did not recover to normal and exhibited black scar (Fig. 6E), while, the skin (Fig. 6E) of mice treated by DMNs almost completely healed, suggesting that PTT through DMNs was a safe modality with good control over elevated temperature at a low-dose ICG (Supporting Information Fig. S8).

The change in mice body weight is a usual indicator to evaluate the safety of formulations. In general, no group showed any noticeable weight loss, albeit, an increasing trend in weight (Fig. 6F), implying that these treatments caused no damage to the mice. Additionally, the H&E staining of various groups (Fig. 7) showed similar results with no lesion and inflammation, which further demonstrated the safety of different treatments.

4. Conclusions

To conclude, HD10 NPs significantly enhanced the cytotoxicity of low-dose PTX by increasing the cellular uptake of NPs and inducing apoptosis *via* the mitochondria. In addition, the combination of chemotherapy and PTT augmented ROS production to facilitate necrosis and the activity of apoptosis-related proteins to induce apoptosis. The HD10 NPs delivered with DMNs in a single administration provided a high efficacy and safe local treatment to the 4T1-bearing tumors. Taken together, the composite DMNs with chemo-photothermal integrated therapy showed favorable anti-cancer effect and great potential in cancer treatment by taking advantage of both NPs and DMNs.

Acknowledgments

Author contributions

Tingting Peng designed the research, performed the experiments, and wrote the manuscript. Yao Huang and Xiaoqian Feng participated part of the experiments. Chune Zhu, Yin Shi, Xinyi Wang, and Xuequn Bai provided data analysis. Xin Pan and Chuanbin Wu revised the manuscript. All authors have read and approved the final version of the article.

Conflicts of interest

The authors have no conflicts of interest to declare.

Appendix A.   Supporting information

Supporting data to this article can be found online at https://doi.org/10.1016/j.apsb.2020.11.013.

References

1. Pandita D, Kumar S, Lather V. Hybrid poly(lactic-*co*-glycolic acid) nanoparticles: design and delivery prospectives. *Drug Discov Today* 2015;**20**:95−104.
2. Bose RJ, Lee SH, Park H. Lipid-based surface engineering of PLGA nanoparticles for drug and gene delivery applications. *Biomater Res* 2016;**20**:34.
3. Danhier F, Ansorena E, Silva JM, Coco R, Le Breton A, Préat V. PLGA-based nanoparticles: an overview of biomedical applications. *J Control Release* 2012;**161**:505−22.
4. Bose RJ, Ahn JC, Yoshie A, Park S, Park H, Lee SH. Preparation of cationic lipid layered PLGA hybrid nanoparticles for gene delivery. *J Control Release* 2015;**213**:92−3.
5. Zheng M, Yue C, Ma Y, Gong P, Zhao P, Zheng C, et al. Single-step assembly of DOX/ICG loaded lipid−polymer nanoparticles for highly effective chemo-photothermal combination therapy. *ACS Nano* 2013;**7**:2056−67.
6. Ma Y, Sadoqi M, Shao J. Biodistribution of indocyanine green-loaded nanoparticles with surface modifications of PEG and folic acid. *Int J Pharm* 2012;**436**:25−31.
7. Rafiei P, Haddadi A. Docetaxel-loaded PLGA and PLGA-PEG nanoparticles for intravenous application: pharmacokinetics and biodistribution profile. *Int J Nanomed* 2017;**12**:935−47.
8. Zhao P, Zheng M, Yue C, Luo Z, Gong P, Gao G, et al. Improving drug accumulation and photothermal efficacy in tumor depending on size of ICG loaded lipid-polymer nanoparticles. *Biomaterials* 2014;**35**:6037−46.
9. Wang G, Yu B, Wu Y, Huang B, Yuan Y, Liu CS. Controlled preparation and antitumor efficacy of vitamin E TPGS-functionalized PLGA nanoparticles for delivery of paclitaxel. *Int J Pharm* 2013;**446**:24−33.
10. Sun Y, Yu B, Wang G, Wu Y, Zhang X, Chen Y, et al. Enhanced antitumor efficacy of vitamin E TPGS-emulsified PLGA nanoparticles for delivery of paclitaxel. *Colloids Surf B* 2014;**123**:716−23.
11. Luo YY, Xiong XY, Cheng F, Gong YC, Li ZL, Li YP. The targeting properties of folate-conjugated Pluronic F127/poly (lactic-*co*-glycolic) nanoparticles. *Int J Biol Macromol* 2017;**105**:711−9.
12. Hu CM, Zhang L, Aryal S, Cheung C, Fang RH, Zhang L. Erythrocyte membrane-camouflaged polymeric nanoparticles as a biomimetic delivery platform. *Proc Nat Acad Sc* 2011;**108**:10980−5.

13. Hu CM, Fang RH, Wang KC, Luk BT, Thamphiwatana S, Dehaini D, et al. Nanoparticle biointerfacing by platelet membrane cloaking. *Nature* 2015;**526**:118−21.

14. Fang RH, Hu CM, Luk BT, Gao W, Copp JA, Tai Y, et al. Cancer cell membrane-coated nanoparticles for anticancer vaccination and drug delivery. *Nano Lett* 2014;**14**:2181−8.

15. Guo R, Peng H, Tian Y, Shen S, Yang W. Mitochondria-targeting magnetic composite nanoparticles for enhanced phototherapy of cancer. *Small* 2016;**12**:4541−52.

16. Chen S, Lei Q, Qiu WX, Liu LH, Zheng DW, Fan JX, et al. Mito-chondria-targeting "nanoheater" for enhanced photothermal/chemo-therapy. *Biomaterials* 2017;**117**:92−104.

17. Souris JS, Lee CH, Cheng SH, Chen CT, Yang CS, Ho JA, et al. Surface charge-mediated rapid hepatobiliary excretion of mesoporous silica nanoparticles. *Biomaterials* 2010;**31**:5564−74.

18. Jiang T, Mo R, Bellotti A, Zhou J, Gu Z. Gel−liposome-mediated co-delivery of anticancer membrane-associated proteins and small-molecule drugs for enhanced therapeutic efficacy. *Adv Funct Mater* 2014;**24**:2295−304.

19. Luo Z, Dai Y, Gao H. Development and application of hyaluronic acid in tumor targeting drug delivery. *Acta Pharm Sin B* 2019;**9**:1099−112.

20. Liu R, Hu C, Yang Y, Zhang J, Gao H. Theranostic nanoparticles with tumor-specific enzyme-triggered size reduction and drug release to perform photothermal therapy for breast cancer treatment. *Acta Pharm Sin B* 2019;**9**:410−20.

21. Chen MC, Lin ZW, Ling MH. Near-infrared light-activatable micro-needle system for treating superficial tumors by combination of chemotherapy and photothermal therapy. *ACS Nano* 2016;**10**:93−101.

22. Dong L, Li Y, Li Z, Xu N, Liu P, Du H, et al. Au nanocage-strengthened dissolving microneedles for chemo-photothermal com-bined therapy of superficial skin tumors. *ACS Appl Mater Interfaces* 2018;**10**:9247−56.

23. Lan X, She J, Lin D, Xu Y, Li X, Yang W, et al. Microneedle-mediated delivery of lipid-coated cisplatin nanoparticles for efficient and safe cancer therapy. *ACS Appl Mater Interfaces* 2018;**10**:33060−9.

24. Pei P, Yang F, Liu J, Hu H, Du X, Hanagata N, et al. Composite-dissolving microneedle patches for chemotherapy and photothermal therapy in superficial tumor treatment. *Biomater Sci* 2018;**6**:1414−23.

25. Yang P, Lu C, Qin W, Chen M, Quan G, Liu H, et al. Construction of a core−shell microneedle system to achieve targeted co-delivery of checkpoint inhibitors for melanoma immunotherapy. *Acta Biomater* 2020;**104**:147−57.

26. Lee IC, He JS, Tsai MT, Lin KC. Fabrication of a novel partially dissolving polymer microneedle patch for transdermal drug delivery. *J Math Chem B* 2015;**3**:276−85.

27. Peng T, Huang Y, Feng X, Zhu C, Ma X, Wang X, et al. Dissolving microneedles loading TPGS biphasic functionalized PLGA nano-particles for efficient chemo-photothermal combined therapy of mel-anoma. *Adv Ther* 2020;**3**:1900190.

28. Zheng C, Zheng M, Gong P, Jia D, Zhang P, Shi B, et al. Indocyanine green-loaded biodegradable tumor targeting nanoprobes for *in vitro* and *in vivo* imaging. *Biomaterials* 2012;**33**:5603−9.

29. Guo Y, Jiang K, Shen Z, Zheng G, Fan L, Zhao R, et al. A small molecule nanodrug by self-assembly of dual anticancer drugs and photosensitizer for synergistic near-infrared cancer theranostics. *ACS Appl Mater Interfaces* 2017;**9**:43508−19.

30. Hu H, Xiao C. Nanocolloidosomes with selective drug release for active tumor-targeted imaging-guided photothermal/chemo combina-tion therapy. *ACS Appl Mater Interfaces* 2017;**9**:42225−38.

31. Shen X, Li T, Chen Z, Xie X, Zhang H, Feng Y, et al. NIR-light-triggered anticancer strategy for dual-modality imaging-guided com-bination therapy *via* a bioinspired hybrid PLGA nanoplatform. *Mol Pharm* 2019;**16**:1367−84.

32. Saxena V, Sadoqi M, Shao J. Degradation kinetics of indocyanine green in aqueous solution. *J Pharmacol Sci* 2003;**92**:2090−7.

33. Wan Z, Mao H, Guo M, Li Y, Zhu A, Yang H, et al. Highly efficient hierarchical micelles integrating photothermal therapy and singlet oxygen-synergized chemotherapy for cancer eradication. *Theranostics* 2014;**4**:399−411.

34. Zheng M, Zhao P, Luo Z, Gong P, Zheng C, Zhang P, et al. Robust ICG theranostic nanoparticles for folate targeted cancer imaging and highly effective photothermal therapy. *ACS Appl Mater Interfaces* 2014;**6**:6709−16.

35. Yan F, Wu H, Liu H, Deng Z, Liu H, Duan W, et al. Molecular imaging-guided photothermal/photodynamic therapy against tumor by iRGD-modified indocyanine green nanoparticles. *J Control Release* 2016;**224**:217−28.

36. Li W, Wang X, Wang J, Guo Y, Lu SY, Li CM. Enhanced photo-acoustic and photothermal effect of functionalized polypyrrole nano-particles for near-infrared theranostic treatment of tumor. *Biomacromolecules* 2019;**20**:401−11.

37. Bershteyn A, Chaparro J, Yau R, Kim M, Reinherz E, Ferreira-Moita L, et al. Polymer-supported lipid shells, onions, and flowers. *Soft Matter* 2008;**4**:1787−91.

38. Chan JM, Zhang L, Yuet KP, Liao G, Rhee JW, Langer R, et al. PLGA-lecithin-PEG core−shell nanoparticles for controlled drug de-livery. *Biomaterials* 2009;**30**:1627−34.

39. Alexis F. Factors affecting the degradation and drug-release mecha-nism of poly(lactic acid) and poly(lactic acid)-*co*-(glycolic acid). *Polym Int* 2005;**54**:36−46.

40. Assanhou AG, Li W, Zhang L, Xue L, Kong L, Sun H, et al. Reversal of multidrug resistance by co-delivery of paclitaxel and lonidamine using a TPGS and hyaluronic acid dual-functionalized liposome for cancer treatment. *Biomaterials* 2015;**73**:284−95.

41. Bao Y, Yin M, Hu X, Zhuang X, Sun Y, Guo Y, et al. A safe, simple and efficient doxorubicin prodrug hybrid micelle for overcoming tumor multidrug resistance and targeting delivery. *J Control Release* 2016;**235**:182−94.

42. Neuzil J, Dong LF, Ramanathapuram L, Hahn T, Chladova M, Wang XF, et al. Vitamin E analogues as a novel group of mitocans: anti-cancer agents that act by targeting mitochondria. *Mol Aspect Med* 2007;**28**:607−45.

43. Neophytou CM, Constantinou C, Papageorgis P, Constantinou AI. D-Alpha-tocopheryl polyethylene glycol succinate (TPGS) induces cell cycle arrest and apoptosis selectively in survivin-overexpressing breast cancer cells. *Biochem Pharmacol* 2014;**89**:31−42.

44. Cerqueira BBS, Lasham A, Shelling AN, Al-Kassas R. Development of biodegradable PLGA nanoparticles surface engineered with hyal-uronic acid for targeted delivery of paclitaxel to triple negative breast cancer cells. *Mat Sci Eng C-Mater* 2017;**76**:593−600.

45. Wang R, Han Y, Sun B, Zhao Z, Opoku-Damoah Y, Cheng H, et al. Deep tumor penetrating bioparticulates inspired burst intracellular drug release for precision chemo-phototherapy. *Small* 2018;**14**: e1703110.

46. Mundra V, Peng Y, Rana S, Natarajan A, Mahato RI. Micellar formulation of indocyanine green for phototherapy of melanoma. *J Control Release* 2015;**220**:130−40.

47. Wang G, Zhang F, Tian R, Zhang L, Fu G, Yang L, et al. Nanotubes-embedded indocyanine green-hyaluronic acid nanoparticles for photoacoustic-imaging-guided phototherapy. *ACS Appl Mater In-terfaces* 2016;**8**:5608−17.

48. Modica-Napolitano JS, Weissig V. Treatment strategies that enhance the efficacy and selectivity of mitochondria-targeted anticancer agents. *Int J Mol Sci* 2015;**16**:17394−421.

49. Zhou J, Zhao WY, Ma X, Ju RJ, Li XY, Li N, et al. The anticancer efficacy of paclitaxel liposomes modified with mitochondrial targeting conjugate in resistant lung cancer. *Biomaterials* 2013;**34**:3626−38.

50. Liang D, Wang AT, Yang ZZ, Liu YJ, Qi XR. Enhance cancer cell recognition and overcome drug resistance using hyaluronic acid and alpha-tocopheryl succinate based multifunctional nanoparticles. *Mol Pharm* 2015;**12**:2189−202.

51. Gialeli C, Theocharis AD, Karamanos NK. Roles of matrix metal-loproteinases in cancer progression and their pharmacological target-ing. *FEBS J* 2011;**278**:16−27.

52. Xu P, Yin Q, Shen J, Chen L, Yu H, Zhang Z, et al. Synergistic inhibition of breast cancer metastasis by silibinin-loaded lipid nanoparticles containing TPGS. *Int J Pharm* 2013;**454**: 21−30.

53. Smit MA, Geiger TR, Song JY, Gitelman I, Peeper DS. A twist-snail axis critical for TrkB-induced epithelial-mesenchymal transition-like transformation, anoikis resistance, and metastasis. *Mol Cell Biol* 2009;**29**:3722−37.

54. Sun XJ, Jin Y, Wang H, Feng N, Li ZH, Liu DD, et al. A NIR-light activated nanoplatform for sensitizing triple negative breast cancer against therapeutic resistance to enhance the treatment effect. *J Math Chem B* 2018;**6**:6950−6.

55. Xu GC, Zhang P, Leng F, Pan L, Li ZY, Yu DD, et al. Inhibition of lymphatic metastases by a survivin dominant-negative mutant. *Oncol Res* 2012;**20**:579−87.

56. Wang H, Wu Y, Zhao R, Nie G. Engineering the assemblies of biomaterial nanocarriers for delivery of multiple theranostic agents with enhanced antitumor efficacy. *Adv Mater* 2013;**25**:1616−22.

57. Zhao X, Li X, Zhang P, Du J, Wang Y. Tip-loaded fast-dissolving microneedle patches for photodynamic therapy of subcutaneous tumor. *J Control Release* 2018;**286**:201−9.

58. Chu KF, Dupuy DE. Thermal ablation of tumours: biological mechanisms and advances in therapy. *Nat Rev Cancer* 2014;**14**:199−208.

59. Yan F, Li L, Deng Z, Jin Q, Chen J, Yang W, et al. Paclitaxel-liposome-microbubble complexes as ultrasound-triggered therapeutic drug delivery carriers. *J Control Release* 2013;**166**:246−55.

60. Zhang L, Wang Y, Yang Y, Liu Y, Ruan S, Zhang Q, et al. High tumor penetration of paclitaxel loaded pH sensitive cleavable liposomes by depletion of tumor collagen I in creast cancer. *ACS Appl Mater Interfaces* 2015;**7**:9691−701.